HHS Public Access

Author manuscript

Mol Cancer Ther. Author manuscript; available in PMC 2021 July 20.

Published in final edited form as:

Mol Cancer Ther. 2020 December ; 19(12): 2528–2541. doi:10.1158/1535-7163.MCT-20-0369.

Implication of *ZNF217* in accelerating tumor development and therapeutically targeting ZNF217-induced PI3K-AKT signaling for the treatment of metastatic osteosarcoma

Branden A. Smeester[#1], **Garrett M. Draper**[#1], **Nicholas J. Slipek**[4], **Alex T. Larsson**[2,4,5], **Natalie Stratton**[1], **Emily J. Pomeroy**[1], **Kelsie L. Becklin**[1], **Kenta Yamamoto**[1], **Kyle B. Williams**[1], **Kanut Laoharawee**[1], **Joseph J. Peterson**[1], **Juan E. Abrahante**[6], **Susan K. Rathe**[5], **Lauren J. Mills**[1], **Margaret R. Crosby**[1], **Wendy A. Hudson**[3], **Eric P. Rahrmann**[7], **David A. Largaespada**[1], **Branden S. Moriarity**[1]

[1]Department of Pediatrics, University of Minnesota

[2]Department of Genetics, Cell Biology, and Development, University of Minnesota

[3]AHCSH Cancer Center, University of Minnesota

[4]Center for Genome Engineering, University of Minnesota

[5]Masonic Cancer Center, University of Minnesota

[6]UMII, University of Minnesota

[7]Cancer Research UK Cambridge Institute, University of Cambridge

[#] These authors contributed equally to this work.

Abstract

We previously identified *ZNF217* as an oncogenic driver of a subset of osteosarcomas (OSAs) using the *Sleeping Beauty* (*SB*) transposon system. Here, we followed up investigating the genetic role of *ZNF217* in OSA initiation and progression through establishment of a novel genetically engineered mouse model (GEMM), *in vitro* assays, orthotopic mouse studies, and paired these findings with preclinical studies using a small molecule inhibitor. Throughout, we demonstrate that ZNF217 is coupled to numerous facets of OSA transformation including proliferation, cell motility, anchorage independent growth, and ultimately promoting OSA growth, progression, and metastasis in part through positive modulation of PI3K-AKT survival signaling. Pharmacological blockade of AKT signaling with nucleoside analogue triciribine (TCN) in ZNF217^{+} orthotopically-injected OSA cell lines reduced tumor growth and metastasis. Our data demonstrate that TCN treatment may be a relevant and efficacious therapeutic strategy for OSA patients with ZNF217^{+} and p-AKT rich tumors. With the recent revitalization of TCN for clinical studies in other solid cancers (PTX-200, Prescient Therapeutics), our study provides rationale for further evaluation preclinically with the purpose of clinical evaluation in patients with incurable, ZNF217^{+} OSA.

Corresponding author: Dr. Branden S. Moriarity, University of Minnesota, Department of Pediatrics, Cancer and Cardiovascular Research Building (CCRB), 2231 6th St. SE, Minneapolis, MN 55455, (e): mori0164@umn.edu, (p): 612-625-4189.

1. Introduction

Osteosarcoma (OSA) is a heterogeneous, rare malignancy of the bone commonly arising in children and adolescents(1). Surgical resection and combinatorial chemotherapy are beneficial to ~70% of localized cases, but patients with advanced metastatic and/or relapsed disease continue to have poor survival outcomes(1,2). Despite remarkable progress in advancing our knowledge of OSA, disease recurrence(3) and chemotherapeutic resistance(4,5) continue to be major roadblocks to curative successes. This significantly underlines the need for new, meaningful therapeutic targets. For these reasons, we performed a *Sleeping Beauty* (*SB*) transposon-based forward genetic screen for OSA which identified >250 previously known and unknown drivers of OSA development and metastasis(6). In particular, zinc finger protein transcription factor (TF) *ZNF217* (murine *Zfp217*) was identified as a candidate OSA driver oncogene in a subset of our primary murine OSA samples(6).

ZNF217 is a member of the Kruppel-like transcription factor family that was originally described with repressive transcriptional function(7). Numerous reports have demonstrated that ZNF217 can influence endogenous signaling networks governing hallmarks of cancer(8,9) including sustained proliferation, invasion/metastasis, and resistance to chemotherapy-induced cell death in other solid tumor types such as ovarian and breast cancer(10–13). This emerging evidence suggests TFs could represent novel candidates for therapy in OSA(14). However, many of these TFs are not currently directly targetable demonstrating the necessity of identifying upstream mediators regulating their biological function.

In this report, we describe a distinct oncogenic role for *ZNF217* in accelerating OSA development, tumor growth, and metastasis in part through transcriptional changes that lead to hyperactivation of PI3K-AKT signaling. Importantly, we show that blockade of AKT signaling with a clinically relevant small molecule inhibitor (triciribine, TCN(15)) is effective at reducing tumor growth and metastasis in $ZNF217^{+}$ tumors. Together, our results suggest continued preclinical evaluation of TCN as a novel therapy for patients with incurable OSA.

2. Materials and methods

RNA expression analyses in OSA data sets

RNA-sequencing was obtained from previously published data available elsewhere(6,16,17) and from the Therapeutically Applicable Research to Generate Effective Treatments (TARGET) initiative, phs000218, managed by the NCI. Information about TARGET can be found at http://ocg.cancer.gov/programs/target.

Detection of copy number variation

Calculated segment means (SM) were obtained and analyzed from 88 OSA samples available within the TARGET initiative using Genomic Suite software (Partek). Cutoff values for categorization were: diploid (SM 1.9 – 2.1), deletion (SM < 1.9), and amplification (SM > 2.1).

Tissue microarray staining (TMA) and analysis

TMA staining and quantification was performed with methods previously described(17). Briefly, two individual OSA TMAs containing 40 samples in duplicate were stained for ZNF217 and p-AKT^{Ser473} respectively and evaluated using the HALO imaging analysis platform (Indica labs). Single cells throughout each TMA section were analyzed for the presence of ZNF217 staining and cellular location (cytoplasm or nucleus were quantified separately via software). Antibodies and other reagents used are available in Supplementary Table 1.

Cell lines and culturing

All OSA cell lines, immortalized osteoblasts (hFOB1.19), and HEK 293Ts were obtained and maintained in accordance with American Type Culture Collection's (ATCC) recommendations. All cell lines were cultured as previously described(17). Normal human osteoblasts (NHOs) were obtained from Lonza and cultured in osteoblast growth medium (#CC-3207, Lonza). With the exception of hFOB1.19 and NHOs, which were recently purchased, other cell lines were authenticated by the University of Arizona Genetics Core (UAGC) using short tandem repeat profiling.

RNAi and overexpression

ZNF217 (#M-004987–00-0005, Dharmacon) and/or control non-silencing (#D-001206–14-05, Dharmacon) pooled siRNAs were used for all transient knockdown studies. OSA cells were transfected at a final working concentration of 17 nM using RNAiMAX (#13778150, Thermo) and all analyses were performed 48 hours post-transfection. Stable knockdown and overexpression of *ZNF217* were achieved with methods previously described(17). Briefly, stable knockdown of ZNF217 was accomplished with pGIPZ lentiviral vectors expressing an shRNA against ZNF217 in conjunction with GFP and a puromycin selection marker (shZNF217: #V2LHS_196547, Open Biosystems). Control pGIPZ vector (shCON) with non-targeting shRNA was used as a control (#RHS4346, Open Biosystems). Stable overexpression (OE) was achieved via a lentiviral *ZNF217* vector (#98384, Addgene) or empty vector control (#41392, Addgene). Lentiviral particles were produced with HEK 293T cells co-transfected with shRNA- or OE-containing vectors, pMD2.G envelope (#12259, Addgene), and psPAX2 (#12260, Addgene) packaging vectors. Viruses were concentrated with Lenti-X (#631232, Clontech) and stable lines were established via puromycin selection at 1 μg/mL following viral transduction.

RT-qPCR

RT-qPCR was performed as previously described(17). Following RNA extraction, 1 μg of total RNA was reverse transcribed into cDNA (#04379012001, Roche) and RT-qPCR was performed in triplicate using SYBR green mix (#4472908, Thermo) on a CFX96 Touch System (Bio-Rad). All measurements were calculated using the ΔΔCT method.

ZNF217 Forward: 5'-GATGTTACTCCTCCTCCGGATG-3'

ZNF217 Reverse: 5'-CACACTTGGCCTGTATCTGCA-3'

ACTB Forward: 5'-CACAGGGGAGGTGATAGCAT-3'

ACTB Reverse: 5'-CTCAAGTTGGGGGCACAAAA-3'

Western blotting

Western blotting was performed as previously described(17). Briefly, total lysates (~20–30 μg) were transferred to PDVF membranes, incubated with 1° and 2° antibodies, developed, and imaged using a LICOR Odyessy. All RNAi and drug experiments were performed for 48 hours prior to western blot analyses. A complete list of antibodies and other reagents utilized is available in Supplementary Table 1.

Immunohistochemistry (IHC)

IHC and H&E staining procedures were performed as previously reported(6). Formalin-fixed and paraffin embedded tissue was sectioned at 4 μM. A complete list of antibodies and other reagents utilized is available in Supplementary Table 1.

Immunofluorescence (IF)

OSA cells (SJSA-1 and HOS) were plated onto sterile glass coverslips and incubated overnight at 37°C in normal media. Cells were washed with PBS and fixed with 10% neutral buffered formalin (NBF) for 10 minutes at room temperature. Following 3X washing with PBS, cells were permeabilized in 0.1% Triton X-100/PBS (#T8787, Sigma Aldrich) for 10 minutes. After 3X washes in PBS, cells were blocked for 1 hour at room temperature in 4% FBS/PBS followed by incubation in 1° antibody/blocking buffer overnight at 4°C. Post-1° incubation, cells were washed 3X in PBS and then incubated in conjugated 2° antibody/blocking buffer for 2 hours at room temperature. Following a gentle PBS wash, antifade mountant containing DAPI (#P36931, Thermo Fisher) was added, coverslips were mounted on glass slides, and imaged using the Cytation 5 cell imaging reader (BioTek). Gen5 software (BioTek) was utilized to acquire and merge IF and DAPI channels. Incubation with 2° only controls yielded no significant IF staining.

Cell fractionation

Cell fractionation (2×10^6 cells/OSA cell line) was performed according to manufacturer's instructions using the subcellular protein fractionation kit for cultured cells (#78840, Thermo Fisher). Equal amounts of total lysate (15 μg) were analyzed via western blot for both OSA cell lines.

Compounds

Both triciribine (TCN, #S1117, Selleckchem) and LY294002 (#S1105, Selleckchem) were prepared according to manufacturer's instructions. Both compounds were dissolved in DMSO for all *in vitro* experiments.

MTS proliferation assay

Cell growth assays were performed as previously described(6,17). Briefly, RNAi-modified cells (1.2×10^3 cells/well) were seeded in 96-well plates. For drug treatment experiments,

cells (2×10^3 cells/well) were incubated for 48 hours with LY294002 or DMSO. Absorbance was measured at 490 nm and 650 nm using a SynergyMx (BioTek) plate reader at 24, 48, 72, and 96 hours post-plating for RNAi experiments and at 48 hours post for LY294002 experiments.

Transwell migration assay

RNAi-modified or TCN-treated cells (2.5×10^4 cells/chamber) were seeded in 500 μL of serum free media in the upper chamber of 8 μm inserts (#353097, Corning). The lower chamber was filled with 750 μL media fortified with 10% fetal bovine serum (FBS) as a chemo attractant. After 24 hours, non-migrating cells where removed with a cotton swab. Migrated cells located on the lower side of the chamber were fixed with crystal violet, air-dried, and photographed to quantify migration of cells.

Soft agar colony formation assay

RNAi-modified or TCN-treated cells (1×10^4 cells/well) were seeded into a 0.35% agar solution placed on top of a 0.5% agar in six-well plates and allowed to incubate for 1–4 weeks. The resultant colonies were fixed, divided into four quadrants, and imaged using microscopy. Colonies were quantified via ImageJ v1.52a software using a standard colony quantification macro(6).

Cell viability assay

OSA cells (2×10^3 cells/well) were seeded into 384-well plates using a Biomek 2000 24 hours prior to experiments. TCN was added in quadruplicate wells per dose in a 12-point two-fold dose-response manner using the acoustic Echo 550 liquid dispenser (Labcyte). At 48 hours post TCN treatment, cells were incubated with alamarBlue reagent (#DAL1100, Thermo Fisher) and fluorescence was read on a CLARIOstar microplate reader (BMG LABTECH). Cell viability was calculated by fluorescence of experimental wells in percent of unexposed control wells with blank values subtracted. Dose-response curves were generated using nonlinear regression log(inhibitor) vs. response-variable slope model.

Flow cytometry

Apoptosis assays were performed as previously described(17). Briefly, cells were resuspended in Annexin-V binding buffer and stained with Annexin-V and 7-AAD according to manufacturer's instructions (#BDB556547, BD Pharmingen). Cells were analyzed on an LSR II or Fortessa digital flow cytometer (BD Biosciences) at the University of Minnesota Flow Cytometry Resource. Analysis was performed using FlowJo software (FlowJo, LLC).

Transgene vector descriptions

A combination of three transgenes were used: 1) osteoblast-specific tetracycline-controlled transactivator (tTA) and Cre-recombinase driven by the Sp7 promoter (*Sp7-tTA,tetO-EGFP::Cre* (abbr. *Sp7-tTA/Cre*); 2) conditionally expressed *Trp53*$^{lslR270H/+}$ dominant-negative (D/N) allele; and 3) tetracycline responsive promoter element (TRE)-driven human *ZNF217* with *Luciferase* reporter (*TRE-hZNF217*-IRES-*Luciferase*; abbr. *TRE-hZNF217/*

Luc). Animals expressing #1 or #2 transgenes outlined above were generated previously and described in detail elsewhere(6). A PB/SB-*TRE-GOI*-IRES-*Luciferase*-based vector(6,17) containing a human *ZNF217* cDNA (Open Biosystems) was generated via the LR cloning system (#11791020, Thermo Fisher) for #3 prior to linearization with SphI (#R0182, New England Biolabs) and pronuclear injection described in the following section.

Pronuclear injection

Transgenic *TRE-hZNF217*-IRES-*Luciferase* mice were generated by University of Minnesota Mouse Genetics Laboratory. C57Bl/6J (Jackson Laboratories) females, 21–28 days of age, were super-ovulated for synchronized fertilized one cell embryo production. Briefly, mice were housed under a 12-hour/12-hour light/dark cycle. Females were injected with 5 international units (IUs) of pregnant mare serum intraperitoneally (IP) at 1:00 PM on day 1. The same females were injected with 5 IUs of human chorionic gonadotropin IP at 12:00 PM on day 3 and immediately mated 1:1 with C57Bl/6J males. Females were checked for copulation plugs on the morning of day 4. Mice with copulation plugs were sacrificed for embryo harvest. Fertilized embryos underwent pronuclear injection on a Leica DM4 microscope. Injected embryos were implanted into 0.5 days post copulation pseudo-pregnant ICR females (Charles River Laboratories), 25 embryos per recipient. Resulting pups were born 19.5 days after implantation. Tail clips were genotyped following weaning at 21 days of age.

Genotyping

Small tail biopsies from weaned animals were collected and genomic DNA was extracted using phenol:chloroform:isoamyl alcohol extraction following overnight digestion in SDS extraction buffer(6). PCR was performed using GoTaq green master mix (#M7121, Promega). Amplicons were resolved on 1% agarose gels and analyzed for the presence of transgenes.

TRE-hZNF217-IRES-*Luciferase* Forward: 5’-TCCAGCTCGACGTTAGAAGG-3’

TRE-hZNF217-IRES-*Luciferase* Reverse: 5’-AGGAACTGCTTCCTTCACGA-3’

Trp53$^{lslR270/+}$ Forward: 5’-TTACACATCCAGCCTCTGTGG-3’

Trp53$^{lslR270H/+}$ Reverse: 5’-CTTGGAGACATAGCCACACTG-3’

Trp53$^{lslR270H/+}$ LSL: 5’-AGCTAGCCACCATGGCTTGAGTAAGTCTGCA-3’

Sp7-tTA,tetO-EGFP::Cre Forward: 5’-CTCTTCATGAGGAGGACCCT-3’

Sp7-tTA,tetO-EGFP::Cre Reverse: 5’-GCCAGGCAGGTGCCTGGACAT-3’

Fluorescence *in situ* hybridization (FISH)

Suspension cultures from fresh mouse spleen cells were initiated: after 48 hours incubation with Concanavalin A, cells were harvested using standard cytogenetic methods (colcemid arrest, followed by treatment with 0.75 M KCl hypotonic solution, and fixation with 3:1 methanol:acetic acid). Harvested cells were spread onto glass slides. ZNF217 DNA probes

were labeled by nick translation reaction (Nick Translation Kit - Abbott Molecular) using Orange 552 dUTP (Enzo Life Science). Sizes of the nick translated fragments are checked by electrophoresis on a 1% TBE gel. The labeled DNA is precipitated in COT-1 DNA, salmon sperm DNA, sodium acetate and 95% ethanol, then dried and resuspended in 50% formamide hybridization buffer. The probe/hybridization buffer mix and slide were denatured, probe was applied to the slide, and slide was hybridized for 48 hours at 37° in a humidified chamber. After hybridization, the FISH slides were washed in a 2xSSC solution at 72° for 15 seconds, and counterstained with DAPI stain. Fluorescent signals were visualized on an Olympus BX61 microscope workstation (Applied Spectral Imaging, Vista, CA) with DAPI and Texas Red filter sets. FISH images were captured using an interferometer-based CCD cooled camera (ASI) and FISHView ASI software.

Bioluminescent imaging

Animals were injected IP with luciferin (#XR-1001, Xenogen) in sterile PBS at 10 μl/g body weight 10–15 minutes prior to imaging. Following administration, animals were gently anesthetized using a mixture of isoflurane and oxygen and imaged using the IVIS 50 *in vivo* bioluminescent system. Functional *Luciferase* imaging was conducted during initial GEMM generation to ensure proper cassette function prior to establishing cohorts.

GEMM tumor detection, localization, and survival analyses

Upon first observation of OSA tumor, time to development was calculated (expressed as % OSA-free survival) and animals were euthanized according to IACUC/institutional regulations. Upon euthanasia, animals were again visually inspected for tumors. Both the number of tumors and location were recorded prior to necropsy.

RNA sequencing and analysis

2 × 75bp FastQ paired end reads (n = 30 million average per sample) were trimmed using Trimmomatic (v0.33) enabled with the optional “-q” option; 3bp sliding-window trimming from 3’ end requiring minimum Q30. Quality control of raw sequence data for each sample was performed with FastQC. Read mapping was performed via Hisat2 (v2.1.0) using the human genome (GRCh38) as a reference. Gene quantification was done via Feature Counts (Subread package) for raw read counts. Differentially expressed genes (DEGs) were identified using the edgeR(17) feature in CLCGWB (Qiagen, Redwood City, CA) using raw read counts. A heatmap was generated using 440 DEGs (fold change +/− 2, FDR < 0.05). STRINGDB (https://string-db.org) was used for pathway enrichment analysis using all DEGs identified. Raw RNA sequencing data from this study are available via GEO (GSE147413).

Orthotopic implantation

All animal procedures were performed in accordance with protocols approved at the University of Minnesota (#1905–37099A) in conjunction with the Institutional Animal Care and Use Committee (IACUC). Wildtype or lentiviral-modified OSA cells (2.5×10^5 in PBS, 20 μL/injection) were implanted through intratibial injection in 6–8-week-old male and female immunocompromised mice (NOD Rag Gamma, Jackson Labs,(18,19)) using a sterile

29-gauge, 0.3 mL insulin syringe (#8881600145, Covidien) just above the calcaneus. Tumor volume was calculated via caliper measurements using the formula V = (W*W*L)/2 where V equals tumor volume, W equals tumor width and L equals tumor length(20). To comply with institutional regulations, all animal experiments were ended when tumor volume approached the 800–1000 mm^3 threshold (post implantation day 31, PID31)

Micro-metastatic lung analysis

Following *in vivo* endpoint (PID 31), whole lungs were subjected to H & E staining. Two slides containing 2–3 lung slices interspaced spaced throughout the whole tissue were made per animal (n = 3/group indicated). A total of 4 representative fields of view were captured per animal and the number of micro-metastatic nodules as well as micro-metastatic area of nodules observed were quantified and averaged (n = 24 images/group indicated).

TCN treatment *in vivo*

Once orthotopic OSA tumors were established (PID 10), animals were randomized and enrolled onto study. Previous clinical research indicated that adult cancer patients received doses of TCN between 20–48 $mg^2/m^2/d$, however; cumulative toxicity was noted in adult patients receiving 30 $mg^2/m^2/d$ (~10 mg/kg/d in mice(21)) despite no toxicities with a 45 mg/m^2 single administration(22). Given the majority of OSA cases are in adolescence(1) and that higher dosages can be required for efficacy in pediatric patients(23,24), we rationalized that a less frequent, higher-dose regimen of TCN may overcome these clinical limitations to date in adults and better serve future pediatric patients. As such, animals received 40 mg/kg TCN or control treatment three times weekly (3X) IP beginning PID 10. TCN was prepared in a 1% DMSO/30% polyethylene glycol/1% Tween-80 solution for all *in vivo* studies.

Statistical analyses

All statistical analyses were performed using Prism v8 software (GraphPad). Two groups were compared using a two-tailed unpaired Student's T-test with or without Welch's correction. Three or more groups were compared using One-way ANOVA or Two-way ANOVA analyses with Bonferroni's post hoc. A log-rank test was utilized for animal survival curve analysis. Simple linear regression analysis was utilized to test for significance between slopes/intercepts. All statistical analyses are individually indicated throughout in figure legends. In all cases, $p < 0.05$ was considered statistically significant.

3. Results

ZNF217 is amplified and ectopically overexpressed in the majority of OSAs examined

Comparative genomics analysis in our previous work uncovered copy number variation (CNV) in *SB*-predicted oncogene *ZNF217* across human OSA samples(6). Further substantiating these findings in a second data set (TARGET) recently made available since our original report, *ZNF217* was found to be amplified in 66% of samples and this amplification positively correlated with increased expression of *ZNF217* (Fig. 1a). Next, we evaluated ZNF217 expression across a series of OSA patient samples in duplicate using immunohistochemical (IHC) staining. Positive ZNF217 staining was detectable in 51.2% of

samples (41/80) (Fig. 1b). As expected, ZNF217 was found in the nucleus of positive cells, but was also detected in the cytoplasm (Figs. 1b–c and Supp. Fig. 1). Likewise, ZNF217 was also found localized in both the nucleus and the cytoplasm of cell lines (Supp. Figs. 2a–b). Lastly, to examine the expression and function of ZNF217 in OSA, we first probed four OSA cell lines for ZNF217 via western blot and compared them to normal human osteoblasts (NHOs). ZNF217 was detectable and aberrantly expressed in all OSA cell lines and not detected in NHOs (Fig. 1d). Overall, this data supports the existence of ZNF217^{+} cells in human samples and OSA cell lines localized in both the nuclear and cytoplasmic compartments.

ZNF217 significantly accelerates tumor formation in an autochthonous mouse model of OSA

Given the fact that a subset of *SB*-mutagenized tumors were driven by *ZNF217* insertions in our previous work(6) and its widespread presence in human tissue samples and cell lines (Fig. 1), we hypothesized that *ZNF217* has an oncogenic role in osteosarcomagenesis. To study this hypothesis, we generated a novel genetically engineered mouse model (GEMM) whereby we achieved osteoblast-specific (*Sp7-tTA,tetO-EGFP::Cre*) expression of human *ZNF217* (*TRE-hZNF217*-IRES-*Luciferase)* and evaluated the capacity of *hZNF217* in osteosarcoma initiation and progression in the presence or absence of an OSA relevant pre-disposing tumor suppressor allele *Trp53*$^{lslR270H/+}$ (Fig. 2a). Positive *TRE-hZNF217*-IRES-*Luciferase* transgene integration was confirmed via FISH (Fig. 2b) and genotyping of all transgenes was confirmed via polymerase chain reaction (Fig. 2c). Functional *Luciferase* expression was validated *in vivo* using bioluminescent imaging (Fig. 2d). Human *ZNF217* overexpression on the *Trp53*$^{lslR270H/+}$ background significantly accelerated OSA development (median 14.3 versus 21.2 months) and penetrance (69% versus 50% versus 0%) as compared to *Trp53*$^{lslR270H/+}$*;Sp7-tTA/Cre* and *TRE-hZNF217/Luc*;*Sp7-tTA/Cre* animals, respectively (Fig. 2e). No OSAs were observed in *TRE-hZNF217/Luc*;*Sp7-tTA/Cre* animals lacking the pre-disposing background (Fig. 2e, blue line). No appreciable difference in the number of OSA tumors per mouse were observed between each genotype (Fig. 2f). 3/12 control animals (25%) had visible macro-metastatic nodules in the lungs (~1–4 individual nodules/animal, in line with our previous report(6)), however no macroscopic metastatic nodules were observed in *TRE-hZNF217/Luc;Trp53*$^{lslR270H/+}$*;Sp7-tTA/Cre* animals. The sites of OSA development were biased to the jaw/cranium (22% versus 8%) and pelvis (22% versus 0%) in *TRE-hZNF217/Luc;Trp53*$^{lslR270H/+}$*;Sp7-tTA/Cre*-expressing animals as compared to control animals (Fig. 2g). These findings were similar to Walkley et al, where facial tumors were the most common site of mouse OSA, which typically had no evidence of metastasis(25). No OSA tumors developed in the pelvis of control animals (left pie graph) and no spinal tumors were present in *TRE-hZNF217/Luc;Trp53*$^{lslR270H/+}$*;Sp7-tTA/Cre*-expressing animals (Fig. 2g). Tumors from experimental animals were positive for human ZNF217 via western blot (Fig. 2h) and were grossly/histologically consistent with OSA via H & E staining(6) (Fig. 2i). In sum, these data indicate that osteoblast specific over expression of *ZNF217* in *Trp53*$^{lslR270H/+}$ predisposed mice leads to accelerated osteosarcomagenesis.

Genetic modulation of *ZNF217* expression significantly alters cellular transformation *in vitro* and OSA tumor growth and metastasis *in vivo*

As expression of human *ZNF217* alone in mouse osteoblasts was not sufficient to initiate OSA development in our GEMM (Fig. 2e, blue line), we deduced that *ZNF217* may be playing a larger role in OSA progression and not tumor initiation. To more closely study this, we adopted a gain/loss-of-function strategy in established OSA cell lines that better mimic facets of cellular transformation involved in tumor progression and metastasis *in vitro* and *in vivo* over our GEMM. Overexpression of *ZNF217* in immortalized osteoblasts and SJSA-1 OSA cells (Fig. 3a) increased cellular proliferation (Fig. 3b). Transient pooled siRNA knockdown of *ZNF217* (Figs. 3c–d) *in vitro* reduced cellular proliferation (Fig. 3e), cellular migration (Fig. 3f), and colony formation in soft agar (Fig. 3g).

With the profound alterations in transformed phenotypes associated with OSA malignancy in *ZNF217* overexpression and knockdown cell lines, we next asked how *ZNF217* expression influences the OSA transcriptome to promote those malignant phenotypes by subjecting SJSA-1 cells to RNA-sequencing following transient *ZNF217* knockdown and analyzing the expression profiles. We obtained a total of 440 differentially expressed genes (DEGs) in our dataset (Supp. Fig. 3a, fold change +/− 2, FDR < 0.05) which consisted of 242 upregulated and 198 downregulated DEGs. All DEGs identified are shown in Supplementary Table 2. A functional protein network coded by all identified DEGs was assembled using STRINGDB (https://string-db.org) (Supp. Fig. 3b). To identify biological attributes and functional categories of the DEGs identified, Gene Ontology (Biological process GO)(26,27) and Reactome(28) pathway analyses were performed on all 440 DEGs altered using STRINGDB. Among the most significantly enriched GO terms were DEGs involved in extracellular matrix organization (ECM), response to stress/stimuli, regulation of cell death, and cell migration (Supp. Fig. 3c). Significant Reactome pathways enriched included ECM organization, collagen modification, integrin signaling, PDGF signaling, and steroid metabolism (Supp. Fig. 3d).

Since metastasis is strongly linked to these phenotypes, we further asked whether *ZNF217* modulates metastasis using SJSA-1 cells with the highest ZNF217 expression (Fig. 1d) *in vivo* following establishment of a stable sh*ZNF217* cell line (Fig. 3h). Similar to our *in vitro* experiments and RNA-sequencing findings, shRNA knockdown of *ZNF217* led to reduced OSA tumor growth (Fig. 3i–j) and metastasis (Figs. 3k–m). Together, these data support a role for *ZNF217* in OSA tumor growth and metastasis.

ZNF217 is associated with regulation of a feedforward loop involving PI3K-AKT signaling

Previous work from Littlepage and colleagues in breast cancer suggests ZNF217 contributes to numerous facets of transformation also important in OSA biology, including epithelial-to-mesenchymal transition, cytoskeletal rearrangement, tumor progression, and metastasis modulated in part through PI3K-AKT signaling (13,29–31). With this is mind, we sought to investigate the PI3K-AKT signaling pathway further in the context of OSA (Fig. 4). PI3K class I catalytic enzymes have been widely implicated in cancer and represent a diverse class with biological and clinical relevance(32). Given this, we correlated *ZNF217* expression with the four class I genes *PIK3CA, PIK3CB, PIK3CD*, and *PIK3CG* and found positive

correlations across all genes in OSA tumor samples combined from two independent data sets (Fig. 4a). In further support, treatment with PI3K inhibitor LY294002 reduced ZNF217 expression (Fig. 4b), reduced cellular proliferation (Supp. Fig. 4a), and induced modest apoptosis (Supp. Fig. 4b). Similar to PI3K class I genes, *ZNF217* also positively correlated with expression of all three AKT isoforms *AKT1*, *AKT2*, and *AKT3* (Fig. 4c). Additionally, active AKT was found to be highly abundant (96.3%) in human OSA samples (Fig. 4d) much like ZNF217 in Figures 1c and 1d, overexpression or knockdown of *ZNF217* increased/reduced p-AKT^{Ser473} in OSA cell lines (Fig. 4e), and gene deficiency led to increased apoptosis similar to PI3K inhibition (Supp. Fig. 5 and Supp. Fig. 4b, respectively). Together, these alterations suggest that ZNF217 promotes a highly invasive and proliferative signaling program that enhances OSA malignancy and metastasis in part through regulation of PI3K-AKT signaling.

Targeted AKT blockade interrupts ZNF217-PI3K-AKT signaling *in vitro*

Transcription factors account for approximately 20% of all oncogenes identified to date and historically have been difficult to drug directly(33). Despite this challenge, recent studies have sought to identify candidate small molecules and miRNA-based therapeutics for combating ZNF217-induced oncogenic signaling, particularly in breast cancer(29). To date, one such compound, triciribine (TCN), has been identified and shown to effectively reduce tumor growth/metastases in ZNF217^{+} breast tumor cells(31) and effective at overcoming Zfp217-induced breast cancer chemotherapy resistance when in combination with paclitaxel(34). We hypothesized that TCN treatment would be an effective therapy for combating the ZNF217-PI3K-AKT positive feedforward loop we identified in OSA cells (Fig. 4). TCN treatment inhibited AKT^{Ser473} and total AKT levels (Fig. 5a), cell viability (Fig. 5b), cellular migration (Fig. 5c), and soft agar colony formation (Fig. 5d). Similar to our PI3K inhibitor studies (Supp. Fig. 4b and Fig. 4b), TCN induced apoptosis (Fig. 5e, Supp. Fig. 6) and reduced ZNF217 expression (Fig. 5f), This data suggests that targeting the PI3K-AKT signaling pathway has robust cytotoxic effects on ZNF217-expressing OSA cell lines treated *in vitro* and that ZNF217 is part of a feedforward loop involving PI3K-AKT signaling.

TCN significantly reduces growth and metastasis in orthotopic OSA tumors

Following our *in vitro* drug studies, we sought to examine the therapeutic potential of TCN in an orthotopic mouse model of OSA using two different OSA cell lines. Tumor-bearing animals were randomized and treated three times weekly (3X) with TCN or control beginning post implantation day 10 (PID 10). Tumor growth was measured until endpoint (PID 31). Tumor volumes were significantly reduced in animals receiving TCN (Fig. 6a). TCN treatment resulted in 5.4- and 3.0-fold changes in average tumor volume at endpoint in animals as compared to control counterparts (SJSA-1 and HOS-injected animals respectively). Similarly, TCN treatment resulted in 2.3- and 2.9-fold reductions in tumor weight at endpoint (Fig. 6b, SJSA-1 and HOS respectively). PD analysis of tumor tissue confirmed that cytoplasmic ZNF217 expression (and to a lesser extent nuclear expression) was reduced in TCN-treated animals (Supp. Fig. 7) similar to our western blot *in vitro* findings (Fig. 5f). TCN treatment was also associated with reduced micro-metastatic nodule

formation and area (Figs. 6c–e). In sum, AKT signaling blockade through TCN treatment effectively reduces ZNF217^{+} OSA tumor growth and metastasis (Fig. 7).

4. Discussion

It is undeniable that novel treatment options are urgently needed for metastatic OSA patients. Here we find that ZNF217 is responsible for the regulation of a feedforward mechanism involving PI3K-AKT signaling that ultimately represents a therapeutically relevant target for significantly reducing OSA tumor growth and metastasis.

We recently identified *ZNF217* (murine *Zfp217*) as a putative driver for a subset of *SB*-induced OSAs(6). Our new autochthonous model of OSA indicates a role for *ZNF217* in the progression, not initiation, of OSA. Encouragingly, other ZNF family members have also been implicated in osteoblastic differentiation(35), facilitating commitment to the osteoblast lineage(36) and were found to be putative drivers in some of our *SB*-induced OSAs(6) (*ZNF592*). *ZNF217* was amplified in 66% of samples examined leading to ectopic oncogenic expression at both the RNA and protein level in OSA tumor samples; observations in line with our inability to detect it in NHOs. Both primary human OSA samples and cell lines had detectable ZNF217 protein in nuclear and cytoplasmic compartments and *ZNF217* was found to be amplified in a significant percentage of OSA samples as previously reported in breast cancer (29,31). Interestingly, cytoplasmic ZNF217 expression has recently been reported in solid tumors of the breast and colon(37,38) and has been functionally linked to estrogen receptor alpha trafficking in MCF-7 breast cancer cells(39,40). In combination with our findings, further investigation into the mechanisms of ZNF217 localization as they relate to OSA tumor development, progression, and metastasis are needed.

Given the role of ZNF217 in OSA progression found in our GEMM, it is not surprising that genetic knockdown of *ZNF217* significantly inhibited hallmarks of cellular transformation, ultimately culminating in reduced OSA tumor growth and metastasis in our orthotopic mouse model. Recent reports suggest that ZNF217 can enhance metastatic bone growth in breast cancer and promote the formation of osteolytic lesions in part through regulation of bone morphogenic protein (BMP) signaling(41,42). BMP signaling has been well-documented in normal bone processes of growth and differentiation(43,44). BMPs are abundant in OSA and have been shown to correlate with metastasis(45,46). This is further supported by complementary reports of oncogenic ZNF217 signaling in colon(47), prostate(48), breast(31), and ovarian(11) solid tumors. Moreover, ZNF217 also protected cells from death, as knockdown readily induced apoptosis. This suggests ZNF217 promotes progression and metastasis in part through regulation of PI3K-AKT survival signaling. Our group and others have demonstrated dysregulated PI3K-AKT signaling can drive a subset of murine(6), canine(49,50), and human OSAs(51–53). This dysregulation is present in a majority of localized OSA cases and in all advanced-stage cases(54,55). Dual reports from Milne et al. and Feng et al. elegantly showed that AKT signaling plays a critical role in murine double minute 2 (MDM2) phosphorylation resulting in protein stabilization and disruption of TP53 signaling(56,57). Mirroring these previous studies, we found correlation between *ZNF217* expression and catalytic PI3K genes as well as downstream *AKT1*, *AKT2*,

and *AKT3* transcripts in OSA patient RNA-sequencing data. Consistent with these findings, we found abundant active AKT staining (p-AKT^{Ser473}) in our OSA TMA. MDM2 is known to interact with ZNF217(58) and is amplified in metastatic OSA(59) suggesting a role for ZNF217-induced PI3K-AKT signaling. Given our identification of PI3K-AKT signaling as a therapeutically targetable axis in ZNF217-expressing OSA cells, these data provide an attractive rationale for investigating small molecule AKT inhibitors preclinically for the treatment of ZNF217^{+} OSAs.

In support of our genetic findings, cytotoxic TCN treatment significantly reduced p-AKT^{Ser473}, phenotypes of cellular transformation *in vitro*, ZNF217 expression, and tumor growth/metastasis *in vivo*. We also found that treatment of OSA cells with PI3K inhibitor LY294002 inhibited cell viability, produced modest apoptosis, and reduced ZNF217 protein expression (unlike a previous report(31)). One possible reason for this discrepancy could be that here we show TCN treatment reduces basal ZNF217 expression, while Littlepage and colleagues examined ZNF217 expression following cell starvation, treatment with TCN, and in the presence of heregulin/neuregulin-1β (See Figure 7D(31)). In sum, this data suggests a positive feedback mechanism for ZNF217-induced AKT signaling which agrees with our overexpression studies that demonstrate strong activation of AKT (p-AKT^{Ser473}) in *ZNF217*-overexpressing immortalized osteoblasts and SJSA-1 OSA cells.

Both Phase I and II clinical trials of TCN have been conducted in advanced malignancies previously(22,60–63). While treatment was associated with some side effects, including hepatotoxicity and hyperglycemia, modest benefits in stabilizing disease were observed in at least one breast cancer patient undergoing treatment(62). A new form of TCN (TCN-P) has been developed (PTX-200, Prescient Therapeutics) and is currently recruiting patients with refractory or relapsed acute leukemia (NCT02930109) and has active status for Phase I treatment of ovarian (NCT01690468) and Phase I/II treatment of stages II-IV breast cancer (NCT01697293) in combination with chemotherapy.

In summary, our data demonstrate a role for ZNF217 in promoting OSA development and orthotopic growth/metastasis through modulation of an oncogenic gene network regulated in part through active PI3K-AKT signaling. Importantly, our work has uncovered the therapeutic potential of targeting the PI3K-AKT signaling axis in OSA through the use of the small molecule AKT inhibitor TCN. Together, this supports the use of TCN in OSA patients with ZNF217^{+} and active PI3K-AKT tumors.

Supplementary Material

Refer to Web version on PubMed Central for supplementary material.

Acknowledgments

The authors would like to thank the Clinical and Translational Science Institute Histology and Research Laboratory team member Dr. Colleen Forester for tissue preparation and histology services. The authors acknowledge the Minnesota Supercomputing Institute, the Institute for Therapeutics Discovery and Development, and the Mouse Genetics Laboratory at the University of Minnesota for providing resources that contributed to the research results reported within this paper. The cytogenetic analyses were performed in the Cytogenomics Shared Resource at the University of Minnesota with support from the comprehensive Masonic Cancer Center NIH Grant #P30 CA077598. Author B.A.S. was previously supported by an NIH NIAMS T32 AR050938 Musculoskeletal Training Grant and is

currently supported by a Doctoral Dissertation Fellowship through the Graduate School at the University of Minnesota. Author G.M.D. is supported by an NIH NIGMS T32 GM113846-09 Stem Cell Biology Training Grant. Author E.J.P. is supported by an NIH NIAID T32 AI997313 Immunology Training Grant. Author K.B.W. is supported by a Children's Tumor Foundation Young Investigator Award from the NF Research Initiative at Boston Children's Hospital made possible by an anonymous gift. This work was made possible through funding from the Zach Sobiech OSA Fund Award, Randy Shaver Cancer and Community Fund, Aflac-AACR Career Development Award, and the Children's Cancer Research Fund to author B.S.M. and American Cancer Society Professor award to author D.A.L.

5. Conflicts of interest

Author D.A.L. is the co-founder and co-owner of several biotechnology companies including NeoClone Biotechnologies, Inc., Discovery Genomics, Inc. (recently acquired by Immunsoft, Inc.), and B-MoGen Biotechnologies, Inc. (recently acquired by bio-techne corporation). He consults for Genentech, Inc., which is funding some of his research. D.A.L. holds equity in and serves as the Chief Scientific Officer of Surrogen, a subsidiary of Recombinetics, a genome-editing company. The business of all these companies is unrelated to the contents of this manuscript. All other authors have no conflicts of interest to disclose.

7. References

1. Kansara M, Teng MW, Smyth MJ, Thomas DM. Translational biology of osteosarcoma. Nature reviews Cancer 2014;14(11):722–35 doi 10.1038/nrc3838. [PubMed: 25319867]
2. Misaghi A, Goldin A, Awad M, Kulidjian AA. Osteosarcoma: a comprehensive review. SICOT J 2018;4:12 doi 10.1051/sicotj/2017028. [PubMed: 29629690]
3. Leary SE, Wozniak AW, Billups CA, Wu J, McPherson V, Neel MD, et al. Survival of pediatric patients after relapsed osteosarcoma: the St. Jude Children's Research Hospital experience. Cancer 2013;119(14):2645–53 doi 10.1002/cncr.28111. [PubMed: 23625626]
4. Yang C, Huang D, Ma C, Ren J, Fu L, Cheng C, et al. Identification of Pathogenic Genes and Transcription Factors in Osteosarcoma. Pathology oncology research : POR 2019 doi 10.1007/s12253-019-00645-w.
5. Zhang Y, Yang J, Zhao N, Wang C, Kamar S, Zhou Y, et al. Progress in the chemotherapeutic treatment of osteosarcoma. Oncol Lett 2018;16(5):6228–37 doi 10.3892/ol.2018.9434. [PubMed: 30405759]
6. Moriarity BS, Otto GM, Rahrmann EP, Rathe SK, Wolf NK, Weg MT, et al. A Sleeping Beauty forward genetic screen identifies new genes and pathways driving osteosarcoma development and metastasis. Nature genetics 2015;47(6):615–24 doi 10.1038/ng.3293. [PubMed: 25961939]
7. Quinlan KG, Verger A, Yaswen P, Crossley M. Amplification of zinc finger gene 217 (ZNF217) and cancer: when good fingers go bad. Biochimica et biophysica acta 2007;1775(2):333–40 doi 10.1016/j.bbcan.2007.05.001. [PubMed: 17572303]
8. Hanahan D, Weinberg RA. The hallmarks of cancer. Cell 2000;100(1):57–70 doi 10.1016/s0092-8674(00)81683-9. [PubMed: 10647931]
9. Hanahan D, Weinberg RA. Hallmarks of cancer: the next generation. Cell 2011;144(5):646–74 doi 10.1016/j.cell.2011.02.013. [PubMed: 21376230]
10. Huang G, Krig S, Kowbel D, Xu H, Hyun B, Volik S, et al. ZNF217 suppresses cell death associated with chemotherapy and telomere dysfunction. Human molecular genetics 2005;14(21):3219–25 doi 10.1093/hmg/ddi352. [PubMed: 16203743]
11. Li J, Song L, Qiu Y, Yin A, Zhong M. ZNF217 is associated with poor prognosis and enhances proliferation and metastasis in ovarian cancer. International journal of clinical and experimental pathology 2014;7(6):3038–47. [PubMed: 25031722]
12. Thollet A, Vendrell JA, Payen L, Ghayad SE, Ben Larbi S, Grisard E, et al. ZNF217 confers resistance to the pro-apoptotic signals of paclitaxel and aberrant expression of Aurora-A in breast cancer cells. Molecular cancer 2010;9:291 doi 10.1186/1476-4598-9-291. [PubMed: 21059223]
13. Vendrell JA, Thollet A, Nguyen NT, Ghayad SE, Vinot S, Bieche I, et al. ZNF217 is a marker of poor prognosis in breast cancer that drives epithelial-mesenchymal transition and invasion. Cancer Res 2012;72(14):3593–606 doi 10.1158/0008-5472.Can-11-3095. [PubMed: 22593193]

14. Morrow JJ, Khanna C. Osteosarcoma Genetics and Epigenetics: Emerging Biology and Candidate Therapies. Critical reviews in oncogenesis 2015;20(3–4):173–97 doi 10.1615/critrevoncog.2015013713. [PubMed: 26349415]
15. Schram KH, Townsend LB. The synthesis of 6-amino-4-methyl-8-(β-D-ribofuranosyl) (4-H,8-H)pyrrolo-[4,3,2-de]pyrimido[4,5-c]pyridazine, a new tricyclic nucleoside. Tetrahedron Letters 1971;12(49):4757–60 doi 10.1016/S0040-4039(01)87546-8.
16. Perry JA, Kiezun A, Tonzi P, Van Allen EM, Carter SL, Baca SC, et al. Complementary genomic approaches highlight the PI3K/mTOR pathway as a common vulnerability in osteosarcoma. Proceedings of the National Academy of Sciences 2014;111(51):E5564 doi 10.1073/pnas.1419260111.
17. Smeester BA, Slipek NJ, Pomeroy EJ, Bomberger HE, Shamsan GA, Peterson JJ, et al. SEMA4C is a novel target to limit osteosarcoma growth, progression, and metastasis. Oncogene 2020;39(5):1049–62 doi 10.1038/s41388-019-1041-x. [PubMed: 31582836]
18. Smeester BA, Al-Gizawiy M, Beitz AJ. Effects of different electroacupuncture scheduling regimens on murine bone tumor-induced hyperalgesia: sex differences and role of inflammation. Evidence-based complementary and alternative medicine : eCAM 2012;2012:671386 doi 10.1155/2012/671386. [PubMed: 23320035]
19. Smeester BA, Al-Gizawiy M, O'Brien EE, Ericson ME, Triemstra JL, Beitz AJ. The effect of electroacupuncture on osteosarcoma tumor growth and metastasis: analysis of different treatment regimens. Evidence-based complementary and alternative medicine : eCAM 2013;2013:387169 doi 10.1155/2013/387169. [PubMed: 24228059]
20. Faustino-Rocha A, Oliveira PA, Pinho-Oliveira J, Teixeira-Guedes C, Soares-Maia R, da Costa RG, et al. Estimation of rat mammary tumor volume using caliper and ultrasonography measurements. Lab animal 2013;42(6):217–24 doi 10.1038/laban.254. [PubMed: 23689461]
21. Nair AB, Jacob S. A simple practice guide for dose conversion between animals and human. J Basic Clin Pharm 2016;7(2):27–31 doi 10.4103/0976-0105.177703. [PubMed: 27057123]
22. Garrett CR, Coppola D, Wenham RM, Cubitt CL, Neuger AM, Frost TJ, et al. Phase I pharmacokinetic and pharmacodynamic study of triciribine phosphate monohydrate, a small-molecule inhibitor of AKT phosphorylation, in adult subjects with solid tumors containing activated AKT. Investigational new drugs 2011;29(6):1381–9 doi 10.1007/s10637-010-9479-2. [PubMed: 20644979]
23. Ivanovska V, Rademaker CM, van Dijk L, Mantel-Teeuwisse AK. Pediatric drug formulations: a review of challenges and progress. Pediatrics 2014;134(2):361–72 doi 10.1542/peds.2013-3225. [PubMed: 25022739]
24. O'Hara K. Paediatric pharmacokinetics and drug doses. Aust Prescr 2016;39(6):208–10 doi 10.18773/austprescr.2016.071. [PubMed: 27990048]
25. Walkley CR, Qudsi R, Sankaran VG, Perry JA, Gostissa M, Roth SI, et al. Conditional mouse osteosarcoma, dependent on p53 loss and potentiated by loss of Rb, mimics the human disease. Genes Dev 2008;22(12):1662–76 doi 10.1101/gad.1656808. [PubMed: 18559481]
26. The Gene Ontology Resource: 20 years and still GOing strong. Nucleic Acids Res 2019;47(D1):D330–d8 doi 10.1093/nar/gky1055. [PubMed: 30395331]
27. Ashburner M, Ball CA, Blake JA, Botstein D, Butler H, Cherry JM, et al. Gene ontology: tool for the unification of biology. The Gene Ontology Consortium. Nature genetics 2000;25(1):25–9 doi 10.1038/75556. [PubMed: 10802651]
28. Fabregat A, Sidiropoulos K, Viteri G, Forner O, Marin-Garcia P, Arnau V, et al. Reactome pathway analysis: a high-performance in-memory approach. BMC Bioinformatics 2017;18(1):142 doi 10.1186/s12859-017-1559-2. [PubMed: 28249561]
29. Cohen PA, Donini CF, Nguyen NT, Lincet H, Vendrell JA. The dark side of ZNF217, a key regulator of tumorigenesis with powerful biomarker value. Oncotarget 2015;6(39):41566–81 doi 10.18632/oncotarget.5893. [PubMed: 26431164]
30. Krig SR, Miller JK, Frietze S, Beckett LA, Neve RM, Farnham PJ, et al. ZNF217, a candidate breast cancer oncogene amplified at 20q13, regulates expression of the ErbB3 receptor tyrosine kinase in breast cancer cells. Oncogene 2010;29(40):5500–10 doi 10.1038/onc.2010.289. [PubMed: 20661224]

31. Littlepage LE, Adler AS, Kouros-Mehr H, Huang G, Chou J, Krig SR, et al. The transcription factor ZNF217 is a prognostic biomarker and therapeutic target during breast cancer progression. Cancer Discov 2012;2(7):638–51 doi 10.1158/2159-8290.Cd-12-0093. [PubMed: 22728437]
32. Fruman DA, Rommel C. PI3K and cancer: lessons, challenges and opportunities. Nature reviews Drug discovery 2014;13(2):140–56 doi 10.1038/nrd4204. [PubMed: 24481312]
33. Lambert M, Jambon S, Depauw S, David-Cordonnier MH. Targeting Transcription Factors for Cancer Treatment. Molecules (Basel, Switzerland) 2018;23(6) doi 10.3390/molecules23061479.
34. Suarez CD, Wu J, Badve SS, Sparano JA, Kaliney W, Littlepage LE. The AKT inhibitor triciribine in combination with paclitaxel has order-specific efficacy against Zfp217-induced breast cancer chemoresistance. Oncotarget 2017;8(65):108534–47 doi 10.18632/oncotarget.19308. [PubMed: 29312549]
35. Twine NA, Harkness L, Kassem M, Wilkins MR. Transcription factor ZNF25 is associated with osteoblast differentiation of human skeletal stem cells. BMC genomics 2016;17(1):872 doi 10.1186/s12864-016-3214-0. [PubMed: 27814695]
36. Qi H, Aguiar DJ, Williams SM, La Pean A, Pan W, Verfaillie CM. Identification of genes responsible for osteoblast differentiation from human mesodermal progenitor cells. Proceedings of the National Academy of Sciences of the United States of America 2003;100(6):3305–10 doi 10.1073/pnas.0532693100. [PubMed: 12631704]
37. Li Z, Du L, Dong Z, Yang Y, Zhang X, Wang L, et al. MiR-203 suppresses ZNF217 upregulation in colorectal cancer and its oncogenicity. PloS one 2015;10(1):e0116170 doi 10.1371/journal.pone.0116170. [PubMed: 25621839]
38. Messana MJ, Yang C, Littlepage LE. Abstract 4252: Regulation of the oncogene ZNF217 by localization in breast cancer. Cancer Research 2014;74(19 Supplement):4252 doi 10.1158/1538-7445.AM2014-4252.
39. Frietze S, O'Geen H, Littlepage LE, Simion C, Sweeney CA, Farnham PJ, et al. Global analysis of ZNF217 chromatin occupancy in the breast cancer cell genome reveals an association with ERalpha. BMC Genomics 2014;15(1):520 doi 10.1186/1471-2164-15-520. [PubMed: 24962896]
40. Nguyen NT, Vendrell JA, Poulard C, Győrffy B, Goddard-Léon S, Bièche I, et al. A functional interplay between ZNF217 and estrogen receptor alpha exists in luminal breast cancers. Mol Oncol 2014;8(8):1441–57 doi 10.1016/j.molonc.2014.05.013. [PubMed: 24973012]
41. Bellanger A, Donini CF, Vendrell JA, Lavaud J, Machuca-Gayet I, Ruel M, et al. The critical role of the ZNF217 oncogene in promoting breast cancer metastasis to the bone. J Pathol 2017;242(1):73–89 doi 10.1002/path.4882. [PubMed: 28207159]
42. Vollaire J, Machuca-Gayet I, Lavaud J, Bellanger A, Bouazza L, El Moghrabi S, et al. The Bone Morphogenetic Protein Signaling Inhibitor LDN-193189 Enhances Metastasis Development in Mice. Frontiers in Pharmacology 2019;10:667. [PubMed: 31275146]
43. Nguyen A, Scott MA, Dry SM, James AW. Roles of bone morphogenetic protein signaling in osteosarcoma. International orthopaedics 2014;38(11):2313–22 doi 10.1007/s00264-014-2512-x. [PubMed: 25209345]
44. Smeester BA, Moriarity BS, Beitz AJ. Osteosarcomagenesis: Biology, Development, Metastasis, and Mechanisms of Pain. Osteosarcoma - Biology, Behavior and Mechanisms2017.
45. Anderson HC, Hsu HH, Raval P, Hunt TR, Schwappach JR, Morris DC, et al. The mechanism of bone induction and bone healing by human osteosarcoma cell extracts. Clinical orthopaedics and related research 1995(313):129–34.
46. Arihiro K, Inai K. Expression of CD31, Met/hepatocyte growth factor receptor and bone morphogenetic protein in bone metastasis of osteosarcoma. Pathology international 2001;51(2):100–6 doi 10.1046/j.1440-1827.2001.01164.x. [PubMed: 11169148]
47. Rooney PH, Boonsong A, McFadyen MC, McLeod HL, Cassidy J, Curran S, et al. The candidate oncogene ZNF217 is frequently amplified in colon cancer. J Pathol 2004;204(3):282–8 doi 10.1002/path.1632. [PubMed: 15476264]
48. Sehrawat A, Gao L, Wang Y, Bankhead A 3rd, McWeeney SK, King CJ, et al. LSD1 activates a lethal prostate cancer gene network independently of its demethylase function. Proceedings of the National Academy of Sciences of the United States of America 2018;115(18):E4179–e88 doi 10.1073/pnas.1719168115. [PubMed: 29581250]

49. Levine RA, Forest T, Smith C. Tumor suppressor PTEN is mutated in canine osteosarcoma cell lines and tumors. Veterinary pathology 2002;39(3):372–8 doi 10.1354/vp.39-3-372. [PubMed: 12014501]
50. Russell DS, Jaworski L, Kisseberth WC. Immunohistochemical detection of p53, PTEN, Rb, and p16 in canine osteosarcoma using tissue microarray. Journal of veterinary diagnostic investigation : official publication of the American Association of Veterinary Laboratory Diagnosticians, Inc 2018;30(4):504–9 doi 10.1177/1040638718770239.
51. Xi Y, Chen Y. PTEN Plays Dual Roles As a Tumor Suppressor in Osteosarcoma Cells. Journal of cellular biochemistry 2017;118(9):2684–92 doi 10.1002/jcb.25888. [PubMed: 28106296]
52. Xi Y, Qi Z, Ma J, Chen Y. PTEN loss activates a functional AKT/CXCR4 signaling axis to potentiate tumor growth and lung metastasis in human osteosarcoma cells. Clinical & experimental metastasis 2020;37(1):173–85 doi 10.1007/s10585-019-09998-7. [PubMed: 31571016]
53. Zhou J, Xiao X, Wang W, Luo Y. Association between PTEN and clinical-pathological features of osteosarcoma. Bioscience reports 2019;39(7) doi 10.1042/bsr20190954.
54. Zhang J, Yu XH, Yan YG, Wang C, Wang WJ. PI3K/Akt signaling in osteosarcoma. Clinica chimica acta; international journal of clinical chemistry 2015;444:182–92 doi 10.1016/j.cca.2014.12.041. [PubMed: 25704303]
55. Zhou W, Hao M, Du X, Chen K, Wang G, Yang J. Advances in targeted therapy for osteosarcoma. Discovery medicine 2014;17(96):301–7. [PubMed: 24979249]
56. Feng J, Tamaskovic R, Yang Z, Brazil DP, Merlo A, Hess D, et al. Stabilization of Mdm2 via decreased ubiquitination is mediated by protein kinase B/Akt-dependent phosphorylation. The Journal of biological chemistry 2004;279(34):35510–7 doi 10.1074/jbc.M404936200. [PubMed: 15169778]
57. Milne D, Kampanis P, Nicol S, Dias S, Campbell DG, Fuller-Pace F, et al. A novel site of AKT-mediated phosphorylation in the human MDM2 onco-protein. FEBS letters 2004;577(1–2):270–6 doi 10.1016/j.febslet.2004.09.081. [PubMed: 15527798]
58. Mantsou A, Koutsogiannouli E, Haitoglou C, Papavassiliou AG, Papanikolaou NA. Regulation of expression of the p21(CIP1) gene by the transcription factor ZNF217 and MDM2. Biochemistry and cell biology = Biochimie et biologie cellulaire 2016;94(6):560–8 doi 10.1139/bcb-2016-0026. [PubMed: 27792410]
59. Ladanyi M, Cha C, Lewis R, Jhanwar SC, Huvos AG, Healey JH. MDM2 gene amplification in metastatic osteosarcoma. Cancer Res 1993;53(1):16–8. [PubMed: 8416741]
60. Feun LG, Blessing JA, Barrett RJ, Hanjani P. A phase II trial of tricyclic nucleoside phosphate in patients with advanced squamous cell carcinoma of the cervix. A Gynecologic Oncology Group Study. American journal of clinical oncology 1993;16(6):506–8 doi 10.1097/00000421-199312000-00010. [PubMed: 8256767]
61. Feun LG, Savaraj N, Bodey GP, Lu K, Yap BS, Ajani JA, et al. Phase I study of tricyclic nucleoside phosphate using a five-day continuous infusion schedule. Cancer Res 1984;44(8):3608–12. [PubMed: 6744283]
62. Hoffman K, Holmes FA, Fraschini G, Esparza L, Frye D, Raber MN, et al. Phase I-II study: triciribine (tricyclic nucleoside phosphate) for metastatic breast cancer. Cancer chemotherapy and pharmacology 1996;37(3):254–8 doi 10.1007/bf00688325. [PubMed: 8529286]
63. Schilcher RB, Haas CD, Samson MK, Young JD, Baker LH. Phase I evaluation and clinical pharmacology of tricyclic nucleoside 5'-phosphate using a weekly intravenous regimen. Cancer Res 1986;46(6):3147–51. [PubMed: 3698029]

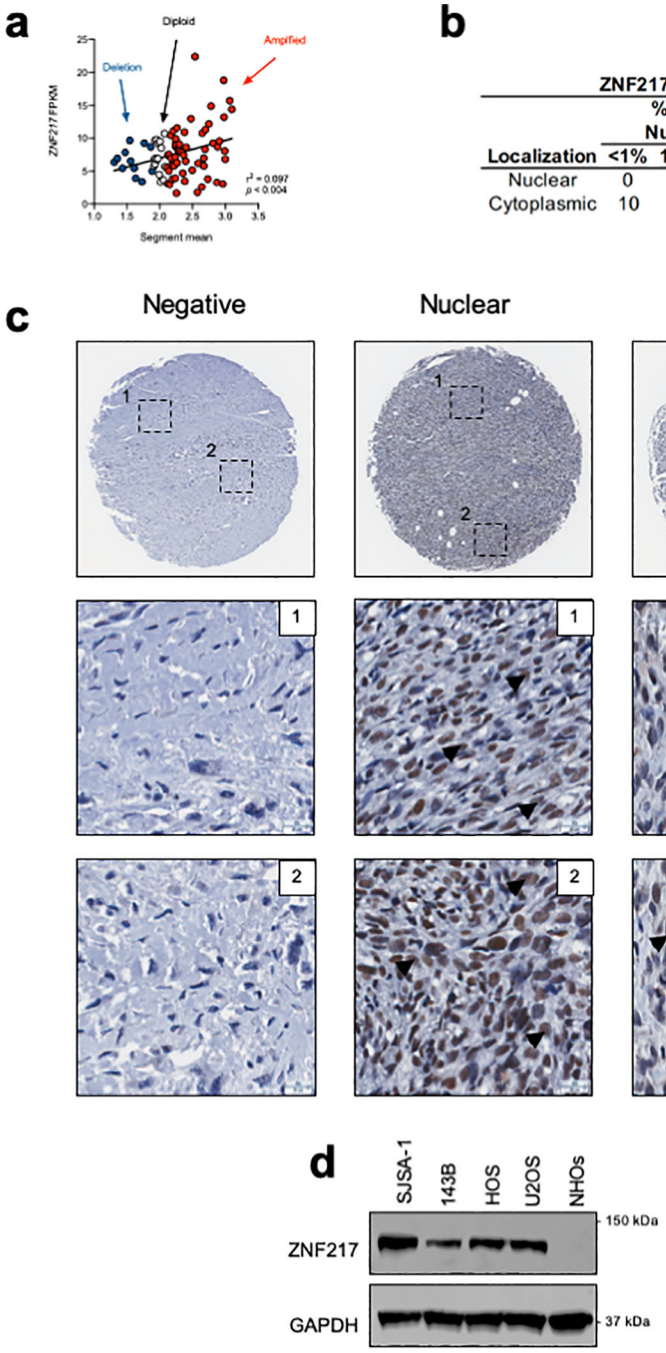

Figure 1. ZNF217 is expressed in OSAs

(a) *ZNF217* CNV and FPKM expression identified in human OSA RNA-sequencing data (n = 88); CNV value = segment mean. (b) Table indicating the number of positive cells at the indicated percentages that express ZNF217 and localization. (c) Images of negative and positive TMA staining for ZNF217 in two representative sites per section; magnification 40X, scale bars 25 μm. Black arrows depict examples of positive nuclear and cytoplasmic ZNF217 staining. (d) Total cell lysates were subjected to western blotting using a ZNF217-specific antibody. Panel (a) Simple linear regression.

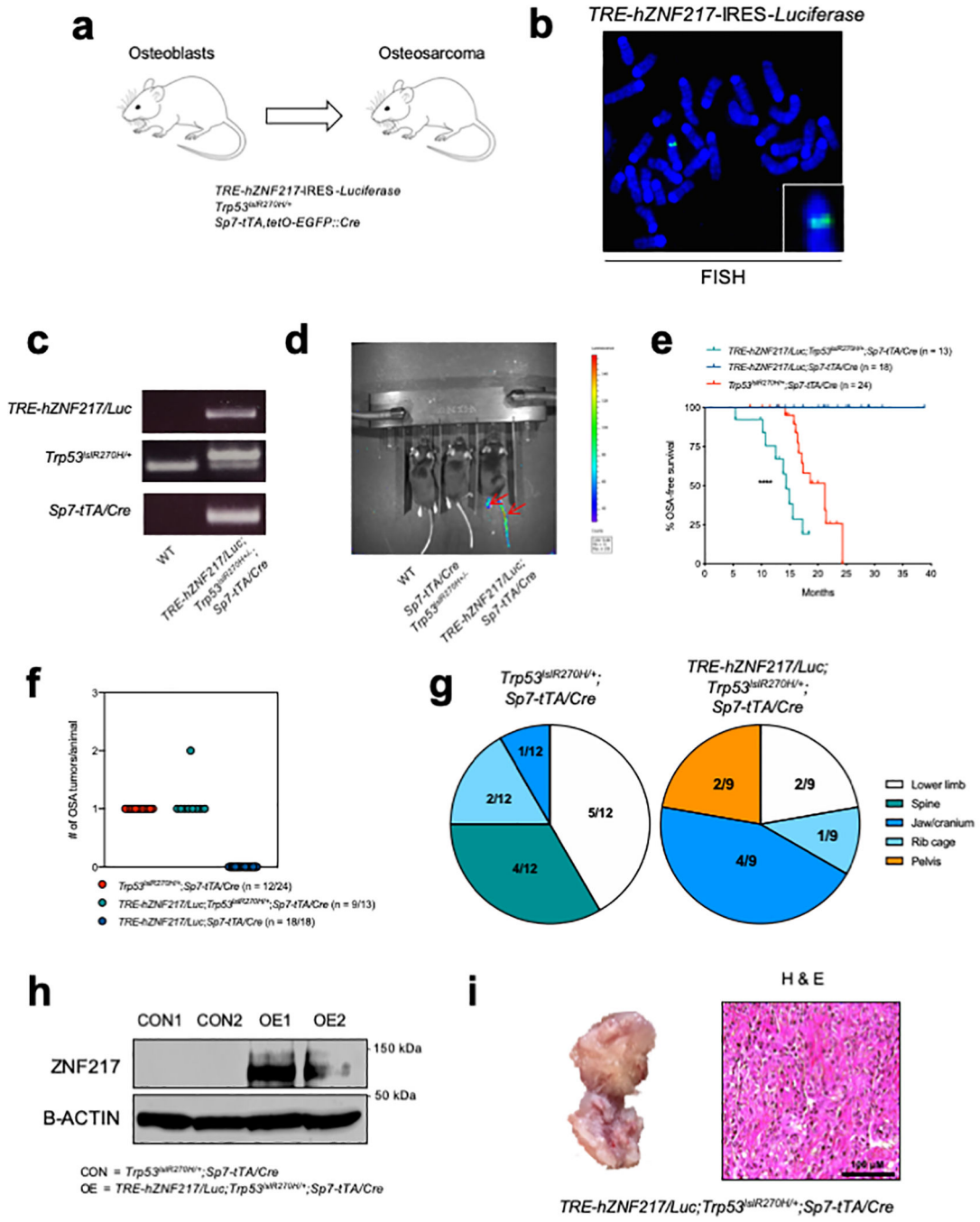

Figure 2. Generation and validation of *ZNF217* genetically engineered mouse model (GEMM)

(a) Breeding schematic used for generating GEMM. (b) Confirmation of *TRE-hZNF217-IRES-Luciferase* transgene cassette integration via FISH. Magnified inset in bottom right corner. (c) Example PCR genotyping confirmation of transgene integrations. (d) Functional validation of positive *Luciferase* expression via bioluminescence in *TRE-hZNF217/Luc;Trp53$^{lslR270H/+}$;Sp7-tTA/Cre* animals. Red arrows indicate positivity. (e) Overexpression of *TRE-hZNF217/Luc; Trp53$^{lslR270H/+}$* in mouse osteoblasts accelerates osteosarcomagenesis. (f) Dot plot of the number of OSAs per animal detected in each

genotype. (g) Distribution of OSA sites observed in indicated genotypes. (h) Total cell lysates from representative tumors were subjected to western blotting using ZNF217-specific antibody. (i) Gross image and representative H & E staining confirming OSA-like appearance in accelerated tumor group; magnification 40X, scale bars 100 μm. Tumor depicted was present on the lower limb. Panel (e) Log rank test. ****$p < 0.0001$.

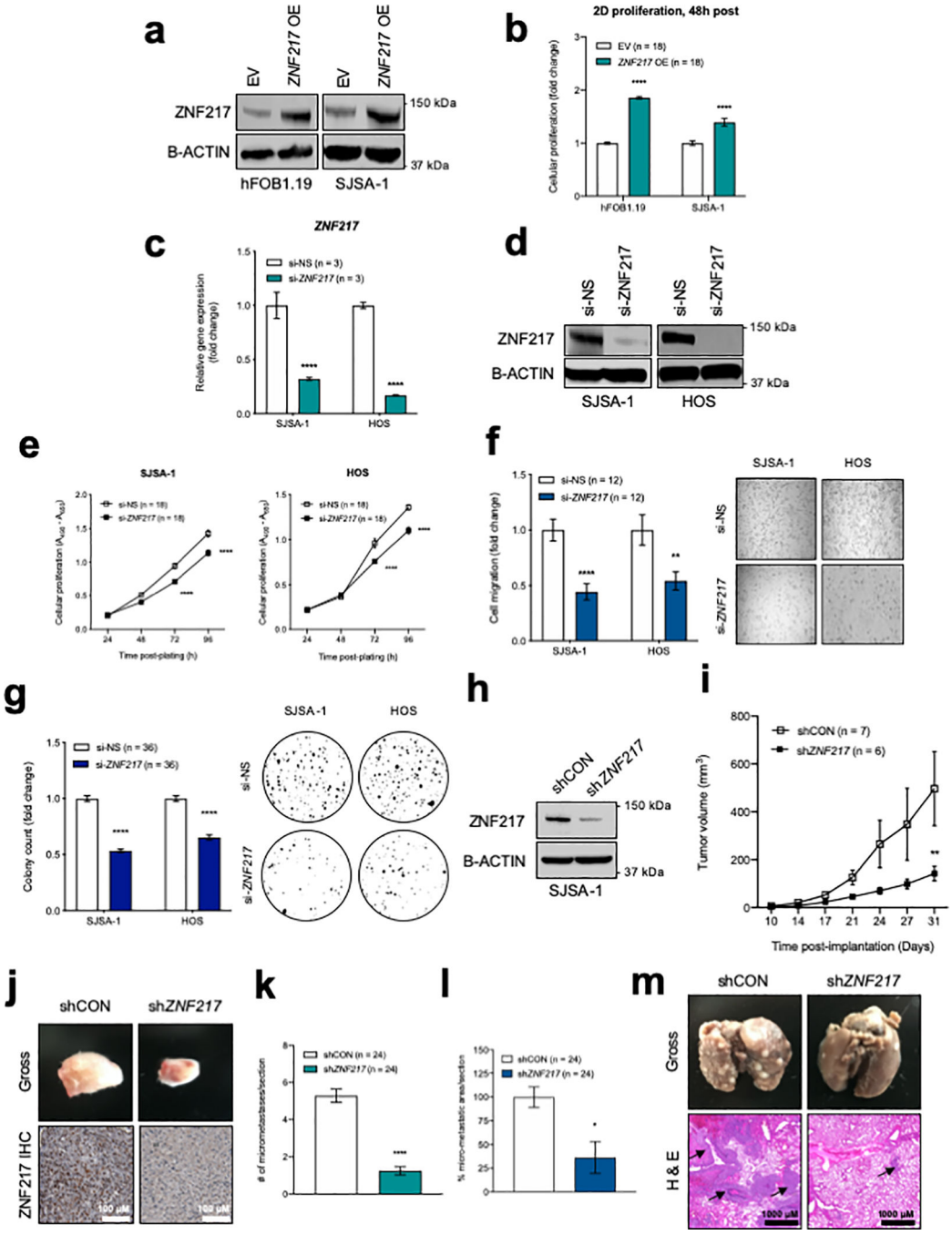

Figure 3. ZNF217 is associated with OSA tumor growth and contributes to metastasis

(a) Confirmation of *ZNF217* overexpression in immortalized osteoblasts (hFOB1.19) and SJSA-1 OSA cells. (b) Overexpression of *ZNF217* increases cell proliferation 48 hours post plating. Confirmation of transient *ZNF217* knockdown via (c) RT-qPCR and (d) western blot. Transient knockdown of *ZNF217* reduces (e) cellular proliferation, (f) migration, and (g) colony formation. (h) Stable *ZNF217* knockdown reduces (i) orthotopic tumor growth. (j) Representative gross tumors and IHC images of ZNF217 in control and knockdown tumors shown to the right; magnification 40X, scale bars 100 µm. (k-l) Stable *ZNF217*

knockdown reduces metastasis. (m) Representative gross lungs and H & E images of control and knockdown tumors shown to the right; magnification 4X, scale bars 1000 μm. Black arrows indicate micro-metastatic nodules. Data shown as mean ± SEM. Panels (b,c,f,g,k,l) Student's T-test. Panels (e,i) Two-way ANOVA with Bonferroni's post hoc. * $p < 0.05$, ** $p < 0.01$, **** $p < 0.0001$.

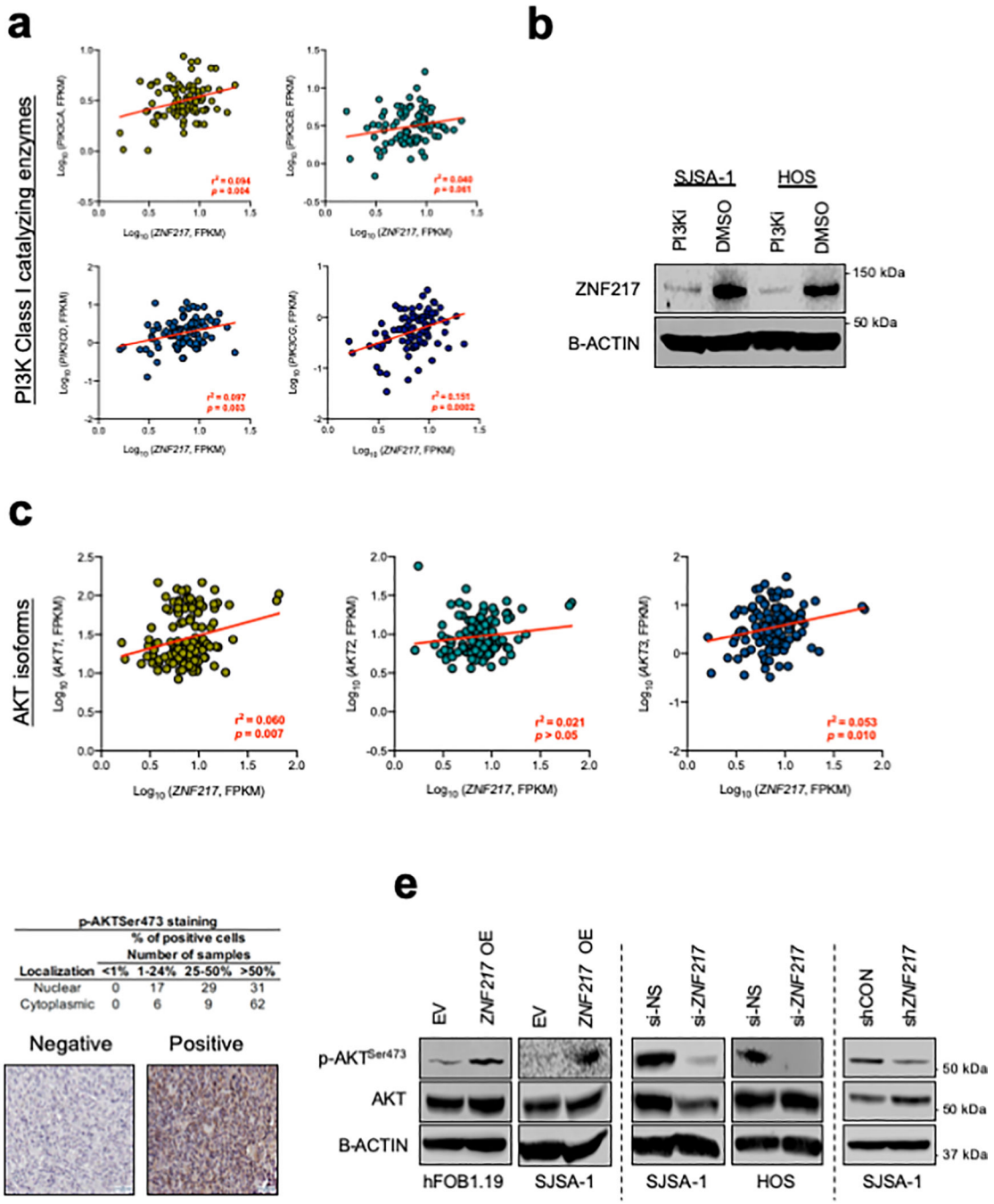

Figure 4. ZNF217 regulates a positive PI3K-AKT signaling loop

(a) *ZNF217* expression is positively correlated with expression of class I PI3K genes in OSA patient data; $\log_{10}$ transformed FPKM values (n = 123). (b) Treatment with PI3K inhibitor LY294002 reduces ZNF217 expression. (c) *ZNF217* expression is positively correlated with expression of *AKT1*, *AKT2*, and *AKT3* in OSA patient data; $\log_{10}$ transformed FPKM values (n = 123). (d) Quantification and representative images of positive and negative p-AKT^{Ser473} staining in a human OSA TMA; magnification 20X, scale bars 50 μm. (e)

Phosphorylation of AKT (p-AKT^{Ser473}) was evaluated after *ZNF217* overexpression and knockdown. Panels (a,c) Simple linear correlation.

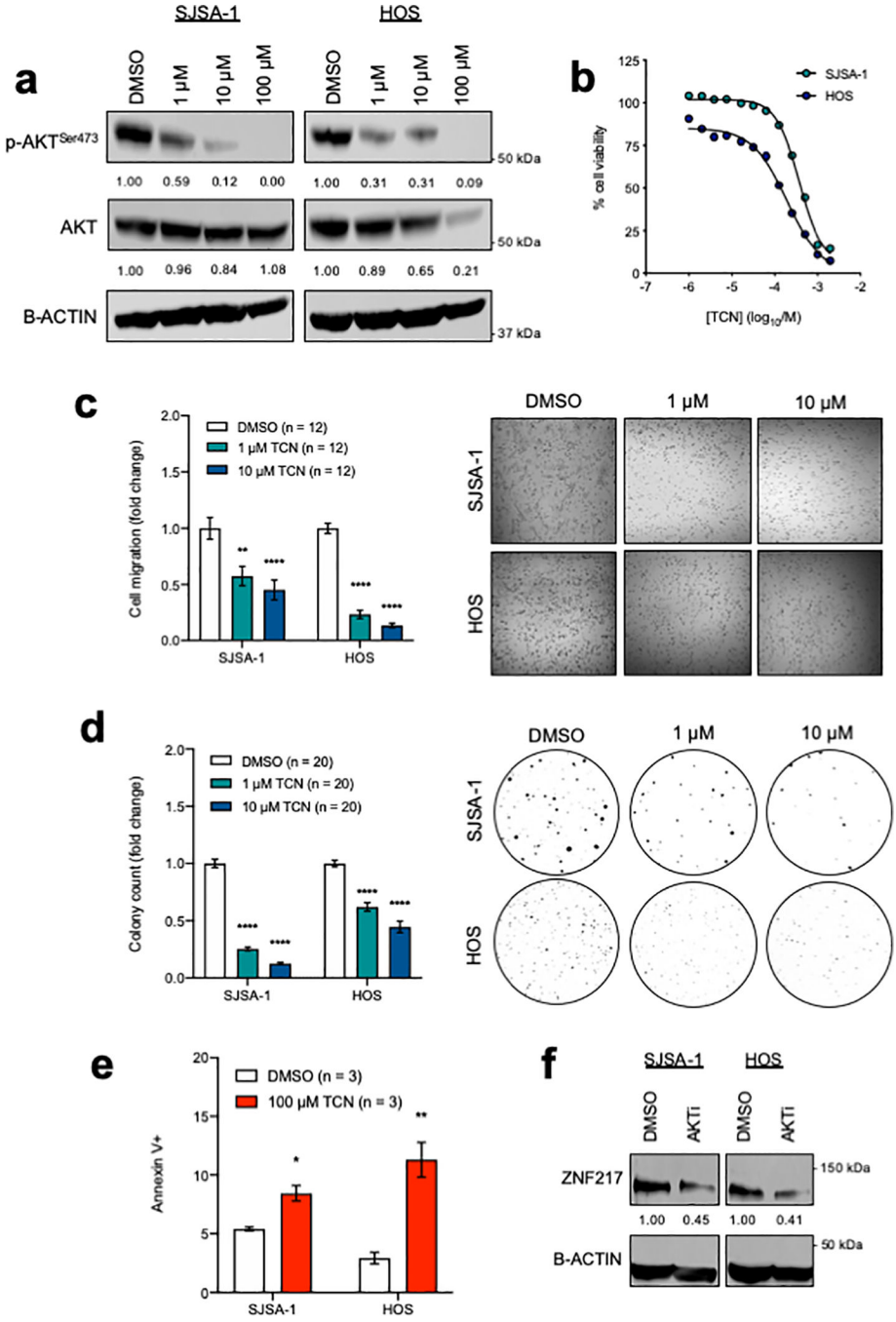

Figure 5. AKT blockade is cytotoxic in OSA cells *in vitro*

(a) A 48-hour treatment with TCN treatment reduces p-AKT^{Ser473}, (b) cell viability, (c) migration, and (d) colony formation. (e) TCN treatment induces apoptosis. (f) Expression of ZNF217 was evaluated after a 48h-hour TCN treatment. Densitometry quantification of western blots show below. All data shown as mean ± SEM. Panels (c,d,e) One-way ANOVA with Bonferroni's post hoc. * $p < 0.05$, ** $p < 0.01$, *** $p < 0.001$, **** $p < 0.0001$.

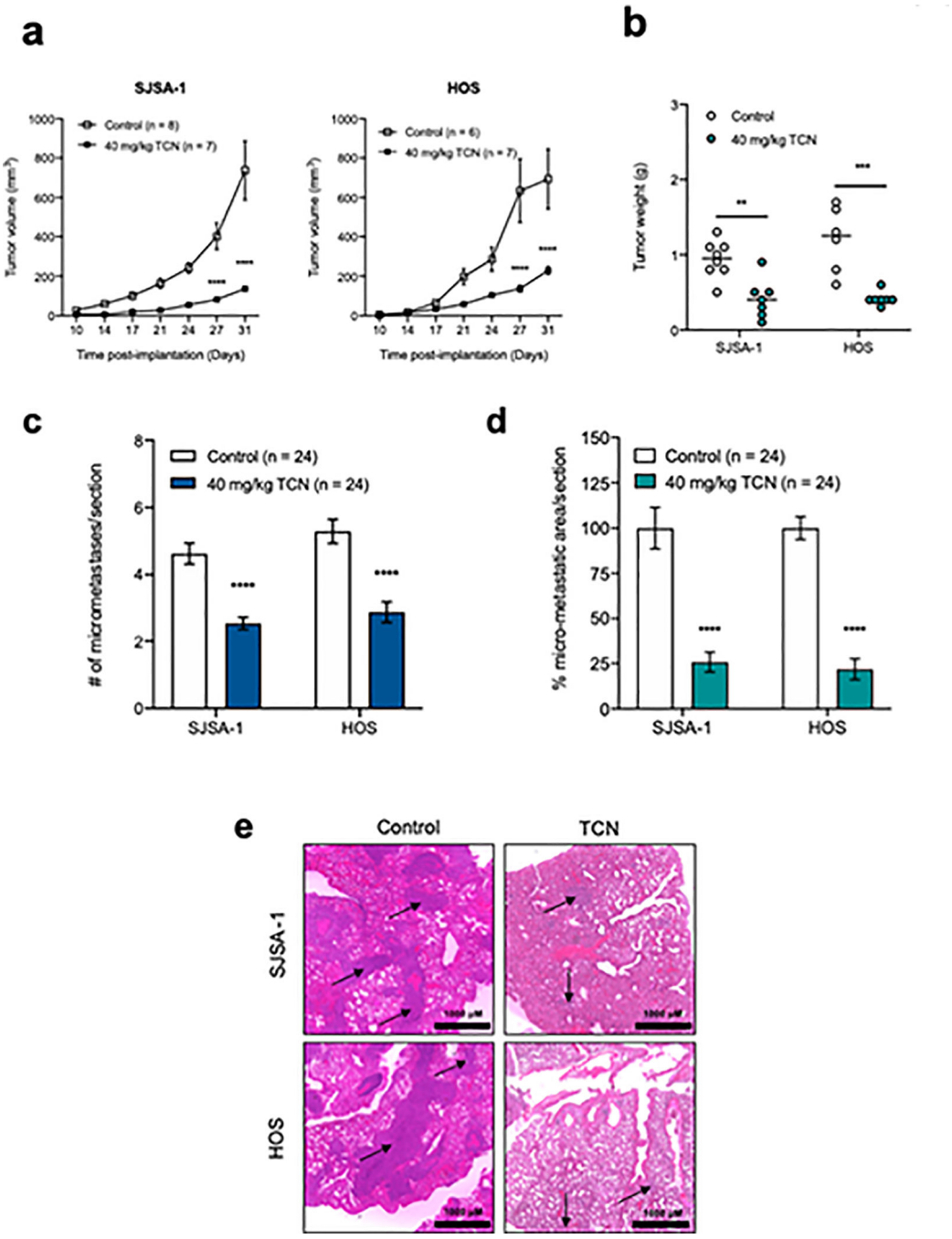

Figure 6. Triciribine effectively reduces orthotopic OSA tumor growth and metastasis

(a) TCN-treated animals displayed reduced tumor growth compared to control-treated animals. (b) TCN treatment reduced tumor weight at endpoint. (c-e) Micro-metastatic burden analysis. Representative H&E staining in lung sections shown to the right; magnification 4X, scale bars 1000 μm. Black arrows indicate micro-metastatic nodules. All data shown as mean +/− SEM. Panel (a) Two-way ANOVA with Bonferroni's post hoc. Panels (b-d) Student's T-test. $^{**}p < 0.01$, $^{***}p < 0.001$, $^{****}p < 0.0001$.

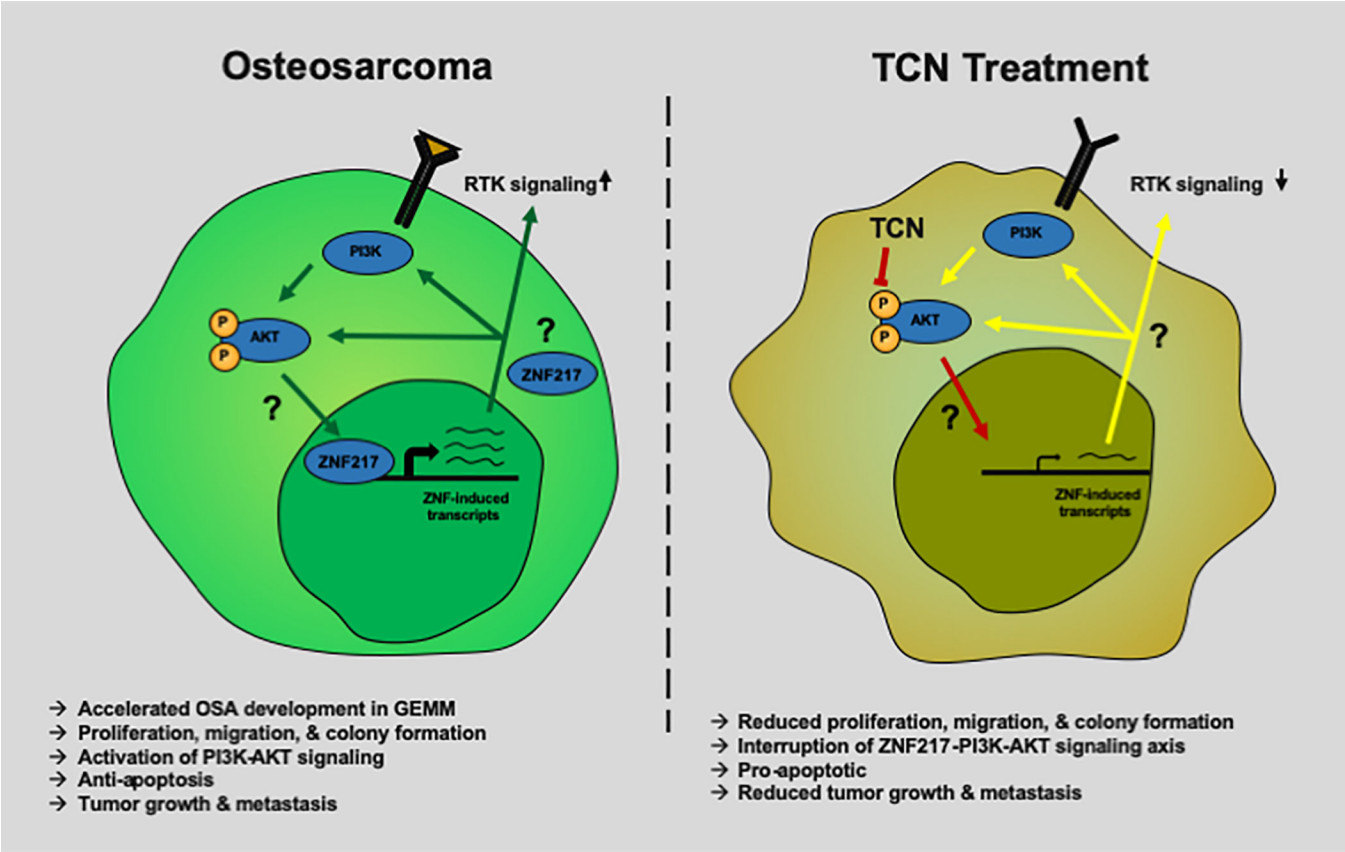

Figure 7. Proposed model for ZNF217-driven PI3K-AKT signaling in OSA and therapeutic targeting

Illustration of model.